Microfluidic preparation and optimization of sorafenib-loaded poly(ethylene glycol-block-caprolactone) nanoparticles for cancer therapy applications

Känkänen, Voitto

2022-11-24

Känkänen , V , Fernandes , M , Liu , Z , Seitsonen , J , Hirvonen , S-P , Ruokolainen , J , Pinto , J F , Hirvonen , J , Balasubramanian , V & Santos , H A 2022 , ' Microfluidic preparation and optimization of sorafenib-loaded poly(ethylene glycol-block-caprolactone) nanoparticles for cancer therapy applications ' , Journal of Colloid and Interface Science , vol. 2023 , no. 633 , pp. 383-395 . https://doi.org/10.1016/j.jcis.2022.11.124

http://hdl.handle.net/10138/353761
https://doi.org/10.1016/j.jcis.2022.11.124

Journal of Colloid and Interface Science 633 (2023) 383–395

Contents lists available at ScienceDirect

Journal of Colloid and Interface Science

journal homepage: www.elsevier.com/locate/jcis

Microfluidic preparation and optimization of sorafenib-loaded poly (ethylene glycol-*block*-caprolactone) nanoparticles for cancer therapy applications

Voitto Känkänen [a,e,*], Micaela Fernandes [a,b,f], Zehua Liu [a], Jani Seitsonen [c], Sami-Pekka Hirvonen [d], Janne Ruokolainen [c], João F. Pinto [b], Jouni Hirvonen [a], Vimalkumar Balasubramanian [e,*], Hélder A. Santos [a,f,*]

[a] Drug Research Program, Division of Pharmaceutical Chemistry and Technology, Faculty of Pharmacy, University of Helsinki, FI-00014 Helsinki, Finland
[b] iMed-ULisboa, Faculty of Pharmacy, University of Lisbon, 1649-003 Lisbon, Portugal
[c] Nanomicroscopy Center, Aalto University, Puumiehenkuja, 2, FI-02150 Espoo, Finland
[d] Department of Chemistry, Faculty of Science, University of Helsinki, P.O. Box 55, 00014 Helsinki, Finland
[e] Drug Carrier and Depot Systems, Bayer Oy, FI-20210 Turku, Finland
[f] Department of Biomedical Engineering, W.J. Kolff Institute for Biomedical Engineering and Materials Science, University Medical Center Groningen, University of Groningen, Ant. Deusinglaan, 1, 9713 AV Groningen, the Netherlands

GRAPHICAL ABSTRACT

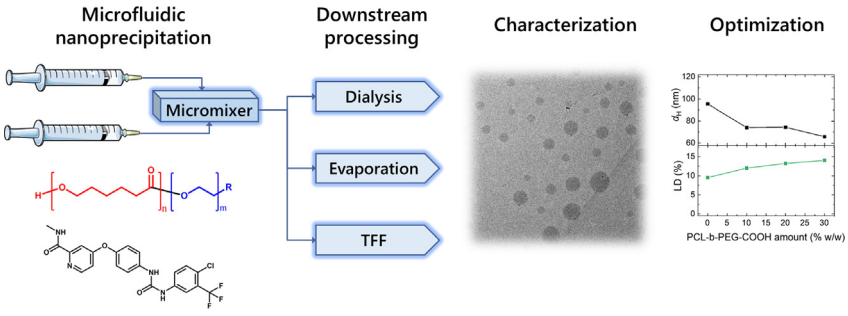

ARTICLE INFO

Article history:
Received 22 October 2022
Revised 9 November 2022
Accepted 23 November 2022
Available online 24 November 2022

Keywords:
Block copolymers
Cancer
Microfluidics
Nanoparticles
Nanoprecipitation
Self-assembly

ABSTRACT

The use of amphiphilic block copolymers to generate colloidal delivery systems for hydrophobic drugs has been the subject of extensive research, with several formulations reaching the clinical development stages. However, to generate particles of uniform size and morphology, with high encapsulation efficiency, yield and batch-to-batch reproducibility remains a challenge, and various microfluidic technologies have been explored to tackle these issues. Herein, we report the development and optimization of poly(ethylene glycol)-*block*-(ε-caprolactone) (PEG-*b*-PCL) nanoparticles for intravenous delivery of a model drug, sorafenib. We developed and optimized a glass capillary microfluidic nanoprecipitation process and studied systematically the effects of formulation and process parameters, including different purification techniques, on product quality and batch-to-batch variation. The optimized formulation delivered particles with a spherical morphology, small particle size (d_H < 80 nm), uniform size distribution (PDI < 0.2), and high drug loading degree (16 %) at 54 % encapsulation efficiency. Furthermore, the stability and *in vitro* drug release were evaluated, showing that sorafenib was released from the NPs in a sustained manner over several days. Overall, the study demonstrates a microfluidic approach to

* Corresponding authors.
E-mail addresses: voitto.kankanen@helsinki.fi (V. Känkänen), vimalkumar.balasubramanian@bayer.com (V. Balasubramanian), h.a.santos@umcg.nl (H.A. Santos).

https://doi.org/10.1016/j.jcis.2022.11.124

produce sorafenib-loaded PEG-*b*-PCL NPs and provides important insight into the effects of nanoprecipitation parameters and downstream processing on product quality.

1. Introduction

The ability of amphiphilic block copolymers (ABCs) to self-assemble into colloidal particles of various morphologies in solution [1] has inspired a vast body of research on their applications as controlled drug delivery systems to improve the treatment of various diseases, with a major focus on cancer [2]. Chemotherapy is an important part of cancer treatment, characterized by severe side effects due to toxicity and limited specificity of the medications. In addition, many anticancer drugs are very poorly soluble in aqueous media, which results in low bioavailability for oral formulations [3], and require the use of solubilizing excipients for intravenous (i.v.) injections, which may cause additional excipient-related side effects [4,5]. The lack of aqueous solubility constitutes a major challenge for the development therapeutic molecules, with up to 90 % of new drug candidates being poorly water-soluble [3].

One strategy to tackle these issues is to solubilize hydrophobic compounds by encapsulation in polymer-based nanoparticles (NPs) [6,7], whence they can be released in a sustained manner *in vivo* after i.v. injection, bypassing the first-pass metabolism by the liver and potentially improving the pharmacokinetic profile by maintaining the concentration of free drug safely within the therapeutic window for extended periods of time [5]. For cancer therapy, additional benefits can be obtained by nanotechnology. For the treatment of certain types of solid tumors, NPs can accumulate preferably at the tumor site by the enhanced permeability and retention effect [8,9] and targeting potential can be further increased by chemical attachment of targeting moieties on the NPs for enhanced accumulation in the diseased tissue [10,11], potentially increasing the treatment efficacy and reducing off-target side effects.

For the preparation of ABC nanoparticles, poly(ethylene glycol) (PEG) and the biodegradable polyester poly(ε-caprolactone) (PCL) are favorable materials due to their widespread use in medical applications and excellent safety profiles [12–18]. The self-assembly of PEG-*b*-PCL in a selective solvent has been shown to generate a variety of interesting NP morphologies, such as spherical micelles, worm-like micelles, vesicles or larger precipitate, typically resulting in a distribution of morphologies as opposed to only a single type [19–22]. However, for drug delivery systems, it is important to have control over the particle morphology and reach a narrow size distribution as these factors are important to treatment safety and efficacy [23,24]. Additionally, reproducibility of manufacturing from batch-to-batch is obviously necessary for industrial translation of any drug delivery system.

Nanoprecipitation method, and different adaptations thereof, have shown great utility in the preparation of nanoparticles for drug delivery applications [25,26]. To further improve this method, micromixers and microfluidic technology have been successfully applied to enable improved control over particle size distribution and drug loading, as well as batch-to-batch reproducibility and scalability [25,27,28]. In particular, glass-based microcapillary devices offer high chemical resistance as well as high thermal stability, low thermal expansion and high heat dissipation capacity compared to devices manufactured from plastics or elastomers [29–31] and have been widely applied in the preparation of nanoparticles for pharmaceutical applications [27,32–36]. The resistance to strong solvents is a key advantage of glass capillary technology, allowing formulation scientists to explore a wider range of raw materials and process conditions to optimize the properties of the final product.

Sorafenib is a multi-kinase inhibitor approved for the treatment of certain liver, kidney and thyroid cancers [37,38]. It is a very poorly water-soluble compound, clinically administered as an oral tablet formulation of its toluenesulfonic acid salt (NEXAVAR), with limited bioavailability [37]. Besides the mentioned indications, it has been studied for a variety of other cancers, including glioblastoma [39–41], breast cancer [42] and melanoma [43] and non-small cell lung cancer [44]. However, the utility of sorafenib for different indications is hampered by poor water solubility, side effects, drug resistance and limited brain penetration, problems which can potentially be ameliorated by advanced nanoformulations. Accordingly, several developments to this direction can be found in the literature [33,36,45–50].

Here, we report the development of sorafenib-loaded block copolymer NPs, for i.v. administration of a model drug, sorafenib. The study is focused on micellar-like PEG-*b*-PCL NPs, in which PCL forms a bioresorbable core [12,51], capable of encapsulating and releasing the hydrophobic drug, and PEG forms a hydrated hydrophilic surface which improves colloidal stability by steric stabilization and increases circulation time *in vivo* [52–54]. We develop and systematically optimize a microfluidic nanoprecipitation process and subsequent purification steps, and study the effect of various process factors on particle size distribution, morphology distribution, zeta (ζ)-potential, drug loading, encapsulation efficiency and process yield. Furthermore, the release of the drug and the stability of the NPs on storage are studied.

2. Experimental

2.1. Materials

Poly(ε-caprolactone)-*block*-poly(ethylene glycol) methyl ether (PCL-*b*-PEG-Me was purchased from PolymerSource, Inc., Canada (Product #P9681-EOCL). Poly(ε-caprolactone)-*block*-poly(ethylene glycol) carboxylic acid (PCL-*b*-PEG-COOH) was purchased from Akina, Inc., USA (Product No AI157). Sorafenib free base (SFB) (>99 %) was obtained from LC laboratories, USA. Chemical structures of the raw materials are shown in **Figure S1**.

Fetal bovine serum (FBS; Gibco) and phosphate-buffered saline concentrate, (10X PBS; HyClone and Cytiva brands), were purchased from Thermo Fisher. Dialysis membrane (50 kDa, Spectra/Por 7 regenerated cellulose) was purchased from Spectrumlabs.com (Repligen). Minimate™ tangential flow filtration (TFF) system was obtained from PALL Corporation. TFF capsules (30 K, Omega™ polyethersulfone membrane) and 0.45 μm Nylon syringe filters (Acrodisc, 13 mm) were purchased from PALL Corporation and 0.45 μm cellulose acetate syringe filters were purchased from VWR.

Acetone (≥99.5 %) was purchased from Sigma. Methanol was purchased from VWR and acetonitrile from Merck. Tetrahydrofuran (THF) used for size-exclusion chromatography was supplied by Honeywell. All solvents were chromatography or reagent grade. Ion-exchange water was obtained using a Milli-Q® Integral 15 Water Purification System with a Millipak® Express 40 filter (Merck Millipore). All other materials were purchased from Sigma.

2.2. Characterization of the block copolymers

Molecular weight distributions of the block copolymers were analyzed by size-exclusion chromatography against polystyrene standards supplied by Polymer Standard Service. Polymers were dissolved in THF and injected into the system consisting of a Waters 515 HPLC pump, Biotech DEGASi GPC Degasser, Waters 717 plus Autosampler, Waters 2487 Dual λ Absorbance Detector and Waters 2410 Differential Refractometer, with Waters Styragel HR1, HR2, and HR4 (7.8 × 300 mm) columns and a guard column.

Chemical compositions of the polymers were analyzed by nuclear magnetic resonance spectroscopy (^{1}H NMR) in $CDCl_3$ using Ascend 400 spectrometer (Bruker) for 64 scans with 1 s relaxation time and analyzed using TopSpin 4.1.1 software. In addition, Fourier-transform infrared spectroscopy (FTIR) was used for chemical characterization of the polymers. Vertex 70 instrument with OPUS 8.1 software (Bruker) and a diamond ATR unit (Pike) were used to collect the absorbance spectra of polymer powders from 600 to 4 000 cm^{-1} at 4 cm^{-1} resolution for 32 scans.

Furthermore, thermal properties of the polymers were analyzed by differential scanning calorimetry (DSC). About 3–4 mg of polymer powder was sealed in aluminium crucibles with pierced lids and analyzed using a DSC823e instrument with STARe 9.00 software (Mettler Toledo). The samples were first heated to + 80 °C and cooled to 0 °C at 10 °C/min under nitrogen to erase previous thermal history and finally heated from 0 to + 80 °C at 10 °C/min under nitrogen to determine the melting temperature.

2.3. Fabrication of the microfluidic device

A heat-resistant micromixer-type co-flow microfluidic device was fabricated from borosilicate glass capillaries and a glass rod (World Precision Instruments, USA), as published elsewhere [55]. For the outer channel, a capillary with 1.50 mm outer diameter and 1.10 m inner diameter was used. For the inner channel, a capillary with inner diameter of 0.58 mm and outer diameter of 1.0 mm was used. One end of the inner capillary was tapered using a micropipette puller (P-97, Sutter instrument co., USA) and the tapered tip was adjusted to an outer diameter of 0.11 mm using fine sand paper. To improve mixing efficiency, a mixing element was prepared using a glass rod with an initial diameter of 1.0 mm, which was given an undulating hourglass-like cross-sectional profile using the same micropipette puller. The capillaries and rods were then assembled co-axially, connected to inlet and outlet ports, and the device was sealed using melted polypropylene. As the molten plastic solidified around the capillaries, it provided a water-tight mechanical seal through thermal contraction. A schematic representation the device cross-section can be seen in **Figure S2**.

2.4. Microfluidic nanoprecipitation method

Nanoparticles were prepared by the microfluidic nanoprecipitation method. A schematic presentation of the process is shown in **Figure S3**. First, the aqueous and organic phases were prepared. Solutions of SFB, PCL-*b*-PEG-Me and PCL-*b*-PEG-COOH at different concentrations were used as organic phases and ion-exchange water or phosphate-buffered saline (PBS) were used as aqueous phases.

During nanoprecipitation, the microfluidic device and approximately 15 cm of the outlet tubing were immersed in a temperature-controlled water bath. Organic phase was injected through the inner capillary and aqueous phase through the outer capillary of the microfluidic device, using disposable plastic syringes (HSW), infusion pumps (PHD 2000, Harvard Apparatus), stainless steel syringe needles and PE-LD tubing (Scientific Commodities, Inc.). Concentrations and process conditions were adjusted for each optimization run. To prevent clogging of the device, a 0.45 μm Nylon syringe filter (Acrodisc, PALL) was applied to the inner phase syringe. Injection was started and after the process had stabilized, NPs were collected and immediately transferred for solvent removal by either dialysis, evaporation or tangential flow filtration (TFF), as detailed later in text. After solvent removal, samples were systematically filtered using 0.45 μm syringe filters (cellulose acetate, VWR).

2.5. Different solvent removal methods

Three different organic solvent removal methods were used in the present study, the details of which are shown below.

a) *Dialysis:* Collected NPs were dialyzed against 1 L of ion-exchange water for 48 h with three water changes (5, 20, 30 h) in a bag of 50 kDa MWCO regenerated cellulose membrane (Spectra/Por) under moderate magnetic stirring.
b) *TFF:* Collected NPs were purified using a Minimate™ TFF system with 30 K Omega™ polyethersulfone membrane filtration cassette (PALL) by filtering against ion-exchange water by discontinuous filtration using two concentration-dilution cycles of 500 mL to 10 mL, resulting in theoretical final acetone concentration of<0.01 % (v/v). Before each run, the system, including the filtration cassette, were flushed with 0.5 L of ion-exchange water. After each run, the system, including the cassette, were systematically washed with 0.2 L of ion-exchange water, 0.2 L of 70 % (v/v) ethanol, 0.2 L of ion-exchange water, 0.2 L of 0.5 M NaOH and finally with 0.1 M NaOH, which was left inside the cassette to prevent microbial growth during cassette storage. The cassette was stored at + 7 °C between experiments.
c) *Evaporation:* Samples were placed in open glass vials and acetone was allowed to evaporate for 24 h under slow magnetic stirring at room temperature.

2.6. Process optimization

The microfluidic process was optimized with respect to seven independent variables: aqueous phase volume fraction during nanoprecipitation, polymer concentration in the organic phase, weight fraction of SFB of the total initial mass of SFB and polymer, weight fraction of PCL-*b*-PEG-COOH of total polymer mass, pH and salt concentration of the aqueous phase, nanoprecipitation temperature and total flow rate expressed as Reynolds number (Re). Re was calculated according to **Eq. (1)**

$$Re = \frac{D v \rho}{\mu} \quad (1)$$

where D is the inner diameter of the outer capillary, ρ is the density of water at 25 °C, v is the linear flow speed calculated from total flow rate and capillary cross-sectional area and μ is the dynamic viscosity of water at 25 °C. Influence of temperature and solvent ratios on density and viscosity were not taken into account.

Ranges of the different variables (**Table S1**) were chosen based on earlier work on the bulk nanoprecipitation of PEG-*b*-PCL [56] and on preliminary drug loading experiments. Full details of each optimization run are listed in **Tables S2 and S3**. The goal of the optimization was to minimize the polydispersity index of NPs and to maximize SFB loading degree, encapsulation efficiency and process yield.

2.7. Particle size distribution and ζ-potential

Particle size distribution and ζ-potential were analyzed by dynamic light scattering (DLS) and electrophoretic light scattering (ELS) methods, respectively, using Zetasizer Nano ZS instrument (Malvern) at 173° scattering angle. Samples were suspended in 0.1X PBS pH 7.4 and filtered using 0.45 μm Nylon syringe filter (Acrodisc, PALL) prior to analysis. All analyses were performed at 25 °C in triplicates.

2.8. Particle morphology

Size and morphology of selected optimization samples were further analyzed by cryogenic transmission electron microscopy (Cryo-TEM). To prepare the specimens, lacey carbon coated copper grids (Electron Microscopy Sciences) were treated with plasma and a drop of NPs dispersion (≈ 1 mg/mL) was applied onto the grids, blotted with filter paper and immersed in liquid ethane using an automatic plunge freezer (EM GP2, Leica). The specimens were stored under liquid nitrogen and imaged at 300 kV using JEM-3200FSC (JEOL) microscope and Digital Micrograph software.

2.9. Loading degree (LD) and encapsulation efficiency (EE)

Sorafenib loading degree (LD) and encapsulation efficiency (EE) and the nanoparticle yield were analyzed by a dry weight method. Aliquots of the dispersions were freeze-dried, weighed and fully dissolved in acetone. Then, SFB concentration was analyzed by high-performance liquid chromatograpy (HPLC, 1260/1100 Infinity series, Agilent) with a C18 column (Gemini NX-C18, Phenomenex) using an isocratic mobile phase of 0.2 % trifluoroacetic acid and acetonitrile (42:58). The LD, EE and yield were calculated according to **Eqs. 2–4**:

$$LD = \frac{Mass\ of\ drug\ in\ NPs}{Mass\ of\ NPs} \quad (2)$$

$$EE = \frac{Mass\ of\ drug\ in\ NPs}{Mass\ of\ drug\ added} \quad (3)$$

$$NPs\ yield = \frac{Mass\ of\ purified\ NPs}{Mass\ of\ raw\ materials\ used} \quad (4)$$

2.10. Stability of NPs in water over storage

To study colloidal stability, NPs dispersion in ion-exchange water (∼1 mg/mL) was divided into aliquots, stored at + 7 °C and + 25 °C and analyzed at 0, 15, 30, 45, 60, 90 and 120 days. Particle size distribution was analyzed by first mixing the samples by vortex and dispersing into 0.1X PBS (pH 7.4), followed by measurement in triplicates, as discussed in section 2.5, without syringe filtration before the measurement. Drug content was measured by first centrifuging the stored samples for 5 min at $(4.0 \times 10^3) \times g$ to remove any possible precipitated non-encapsulated drug or agglomerated particles, followed by mixing the supernatant with acetone (1:19) to dissolve the NPs and analyzing the SFB concentration using a method described in 2.9.

2.11. Sorafenib solubility

Aqueous solubility of SFB was determined in buffers at pH 3.9–7.4 with and without supplementation of the buffer with 10 % v/v FBS. 0.1 M acetate buffers at pH 3.9, 4.6 and 5.3 and 1X PBS buffers at 6.0, 6.7 and 7.4 were used. An excess of drug powder was mixed in a glass vial with the dissolution medium and stirred at + 37 °C overnight. Three independent vials were prepared for each dissolution medium. Undissolved drug powder was then removed by centrifugation for 15 min at $2.0 \times 10^4 \times g$ at + 37 °C, samples were carefully collected from supernatants, diluted 1:1 with methanol and analyzed by HPLC using the method shown in 2.9.

2.12. Sorafenib release rate in vitro

Release rate of SFB from the PEG-*b*-PCL NPs was analyzed by the dialysis bag method [57]. PBS buffers at pH 7.4 and pH 5.5, supplemented with 10 % (v/v) FBS were used as the dissolution media. To ensure sink conditions (as discussed in section 3.7), 400 mL of the release medium was used and the amount of drug inside the dialysis bag was limited to 25 ± 2 μg. To illustrate the finite permeation rate and equilibration time inherent to the dialysis method, a simple solution of SFB in poly(ethylene glycol) 400 (PEG400) and ion-exchange water (1:1) was prepared and used as a control sample.

To start the experiment, 3.5 mL of NP dispersion or the control solution was placed inside a dialysis membrane bag (50 kDa MWCO) and immersed in the release medium at + 37 °C under moderate magnetic stirring. Samples of 2.0 mL were drawn from the release medium at time points of 0.5, 1, 2, 4, 8, 24, 48 and 72 h and replaced with equal volumes of fresh medium. To reach quantifiable concentrations, SFB was extracted from the samples twice with diethyl ether (≥97.5 %, Aldrich) (2 × 3.5 mL), the ether was evaporated and the dry samples dissolved in 0.25 mL of methanol. Finally, the samples were analyzed by HPLC, as shown in section 2.9.

At the end of each experiment, the amount of SFB remaining inside the dialysis bag was quantified. Firstly, the contents of the bag were collected and the bag was rinsed with a small amount of water. The collected liquid, including the rinsing liquid, was freeze-dried. To the dry samples, 2.0 mL of methanol was added and the samples were mixed carefully by three alternating cycles of vortex mixing (10–15 s) and tumbling (10–15 s), followed by a final 10–15 s vortex mixing, after which extraction was allowed to occur for ∼ 2 h at room temperature. Finally, the samples were centrifuged for 10 min at $1.6 \times 10^4 \times g$ and the supernatants were analyzed by HPLC, as detailed above.

3. Results and discussion

3.1. Characterization of the block copolymers

Results from polymer characterization are shown in Fig. 1. FTIR spectra of the two polymers were almost identical and important absorption bands could be seen at 1722 cm^{-1} (PCL, carbonyl C═O stretch), 2945 and 2864 cm^{-1} (C—H stretch), 1177 cm^{-1} (PEG, C—O—C stretch) and 1240 cm^{-1} (PCL, COO stretch). These results are in accordance with the PEG-*b*-PCL structure, as was also reported elsewhere [58]. Based on *SEC* data, the number-average molecular weights of the block polymers were determined to be 1.14×10^4 g/mol at Đ = 1.26 for PEG-*b*-PCL-Me and 1.23×10^4 g/mol at Đ = 1.28 for PEG-*b*-PCL-COOH. By comparing the integrated areas of PEO protons (3.6 ppm) and PCL protons (4.1 ppm) in NMR spectra, the weight fraction of PEO was calculated to be χ_{PEO} = 0.162 for PCL-*b*-PEG-Me and χ_{PEO} = 0.166 for PCL-*b*-PEG-COOH. Neither FTIR nor ^{1}H NMR were sensitive enough to verify the presence of the singular carboxylic end group of PCL-*b*-PEG-COOH. DSC data showed a melting event at + 54.4 °C for PCL-*b*-PEG-Me and + 54.8 °C for PCL-*b*-PEG-COOH. Slightly higher melting point for PCL-*b*-PEG-COOH may be explained by the higher molecular weight. All results were in good agreement with supplier batch data, and indicate that no significant hydrolysis of the polymers had occurred during storage.

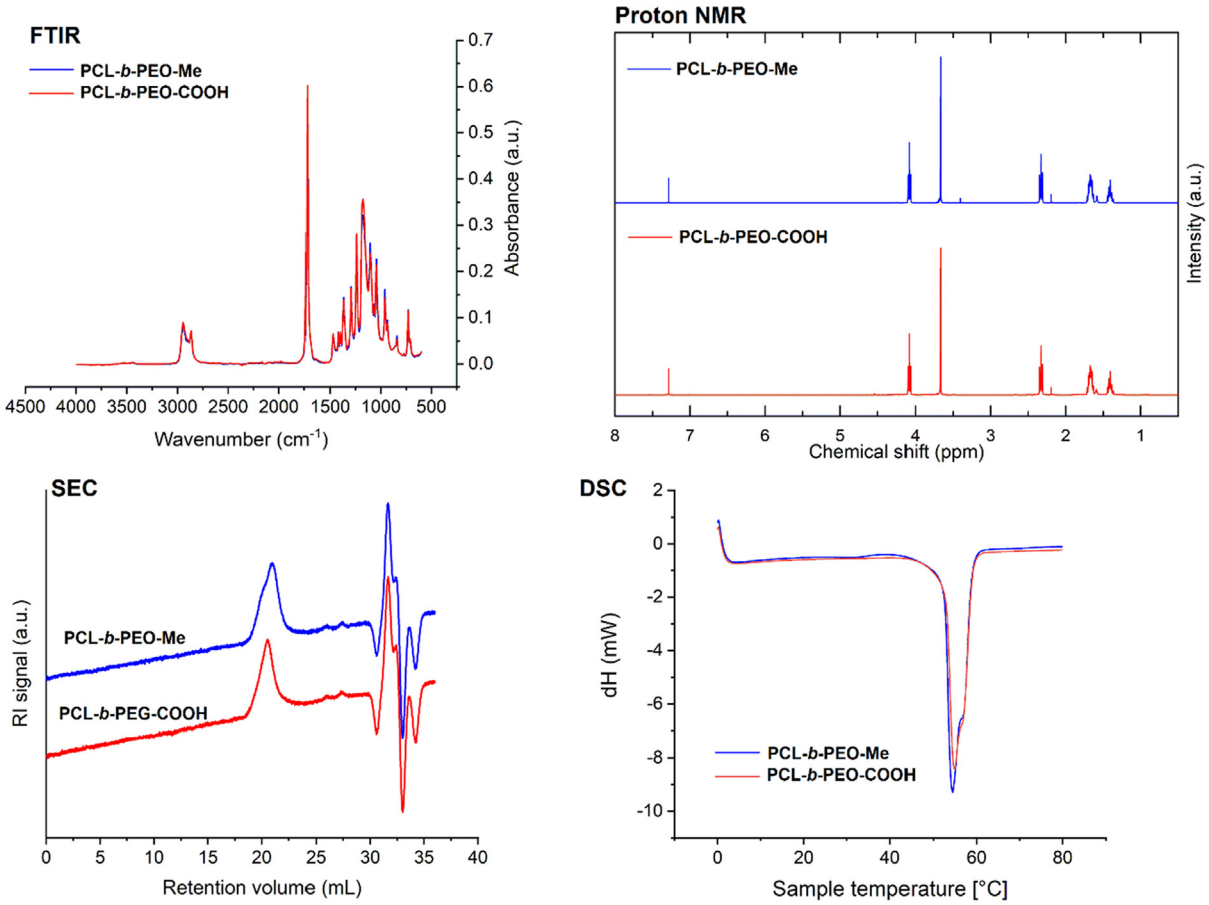

Fig. 1. The block copolymers were characterized by FTIR, ^{1}H NMR, *SEC* and DSC methods.

3.2. Effects of formulation and microfluidic process parameters: Dialysis-based solvent removal experiments

To optimize the microfluidic process, the effects of seven formulation and process parameters on product properties (particle size, PDI, ζ-potential, loading degree and encapsulation efficiency) were explored. For each optimization run, 4.0 mL of the NP dispersion was prepared by the microfluidic method and purified using dialysis and syringe filtering as detailed above.

3.3. Effects of formulation and process parameters on particle size distribution and ζ-potential

The optimization results with respect to d_H, PDI and ζ-potential and particle morphology are shown in Figs. 2-4. As seen in Fig. 2A, increasing the amount of PCL-*b*-PEG-COOH from 0 to 30 % reduced strongly the mean d_H (from 91.0 ± 0.5 nm to 65.9 ± 1.0 nm) and PDI (from 0.174 ± 0.005 to 0.141 ± 0.005). This can be explained by the electrostatic repulsion of the negatively charged hydrophilic blocks and its effect on block polymer self-assembly. In order to maximize the distance between ionized PEG end groups, structures of higher surface curvature, and thus, lower PEG tethering density per unit area are favored, which results in small spheres as opposed to larger particles, worm-like or bilayer structures [59]. Indeed, examination of samples (Runs 16 and 20, **Table S2**) by Cryo-TEM confirmed that the addition of COOH-functionalized polymer reduced the amount of worm-like and lamellar structures and favored a spherical morphology (Fig. 3). Corresponding low-magnification micrographs are available in **Figure S4** for a better overview of the obtained morphologies. The results indicate that a more homogeneous morphology distribution was obtained at 30 % of PCL-*b*-PEG-COOH.

Fig. 2B shows that also the salt concentration of the aqueous phase had a significant effect on the particle size distribution, but did not affect the ζ-potential. For example, when PBS (pH 7) was used as the aqueous phase, larger particles (89.0 ± 0.4 nm at PDI 0.163 ± 0.006) were obtained as opposed to when using water (71.9 ± 0.3 nm at PDI 0.126 ± 0.007). This salt effect can be explained by shielding of the deprotonated – COOH-groups by the salt ions [59], which reduces the effect of electrostatic repulsion of the corona-forming chains, as discussed above. The effect of aqueous phase pH was small within the narrow pH range studied. Increasing the polymer concentration appeared to slightly reduce the mean d_H, with no significant effect on PDI or ζ-potential (Fig. 2C). This can be explained by an increased supersaturation level of polymer, leading to formation of larger amounts of stable nuclei [25].

Increasing drug feed (Fig. 2D) caused a slight increase in d_H (from 69.9 ± 0.3 nm at 0 % to 73.6 ± 0.5 nm at 25 % drug feed), which can be explained by increased drug loading per particle, whereas no significant effects on PDI or ζ-potential were observed. Within the studied range, water fraction during nanoprecipitation had no significant effects on d_H, PDI or ζ-potential (Fig. 2E). The size distribution data is consistent with our previous findings using the bulk nanoprecipitation method, showing that within values of approximately 55 to 87.5 %, water fraction does not significantly affect the particle size distribution for this polymer [56].

Fluid flow rate had a significant effect on d_H and PDI (Fig. 2F), with larger values obtained at low Re (*e.g.*, d_H = 85.2 ± 0.2 nm and PDI = 0.189 ± 0.004 at 2 Re) and smaller values obtained at high

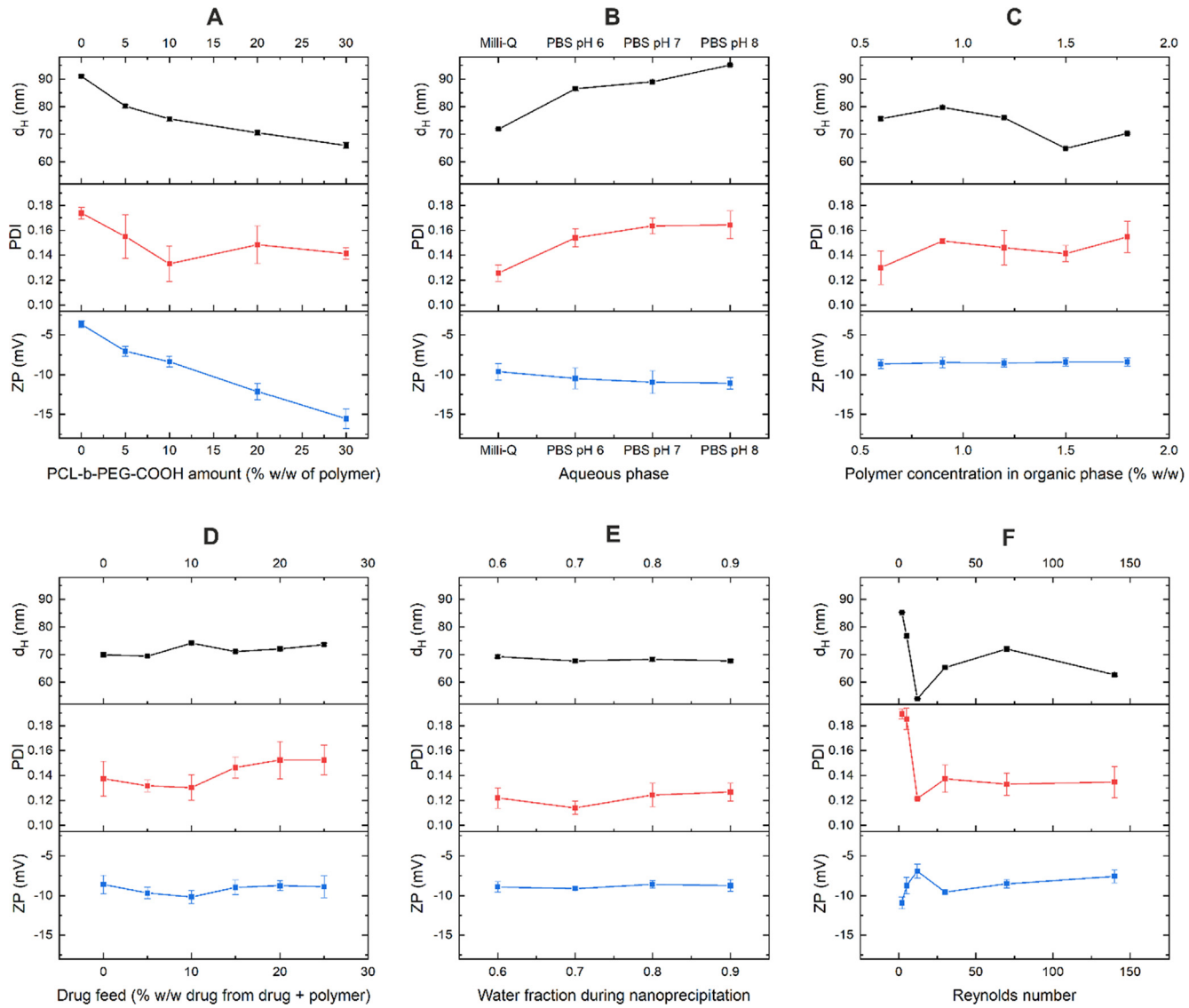

Fig. 2. Effects of the formulation and process parameters on average hydrodynamic diameter (d_H), polydispersity index (PDI) and zeta (ζ)-potential (ZP) at pH 7.4. Results are from single batches per condition, each analyzed in triplicates.

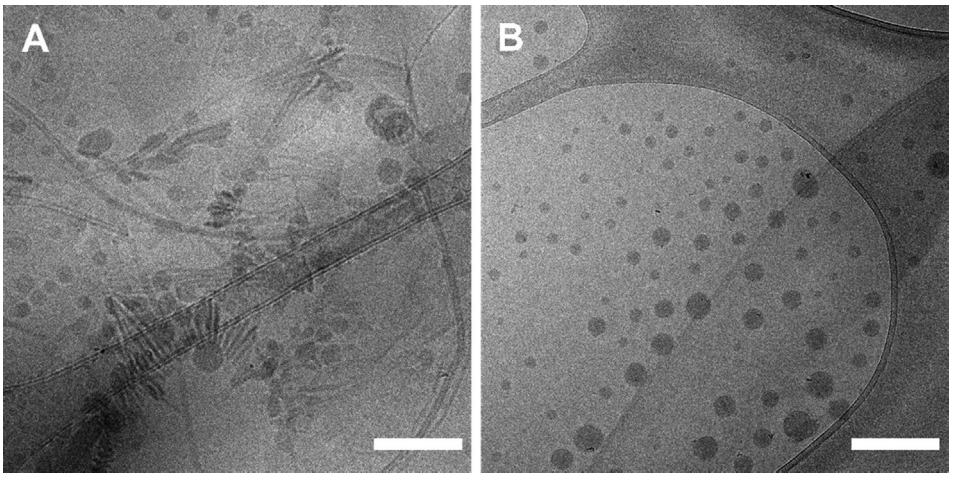

Fig. 3. Cryo-TEM micrograph of PCL-*b*-PEG NPs prepared (A) without PCL-*b*-PEG-COOH and (B) with 30 % of PCL-*b*-PEG-COOH. Scale bars are 200 nm. See Fig. S4 in Supplementary information for the respective low-magnification micrographs.

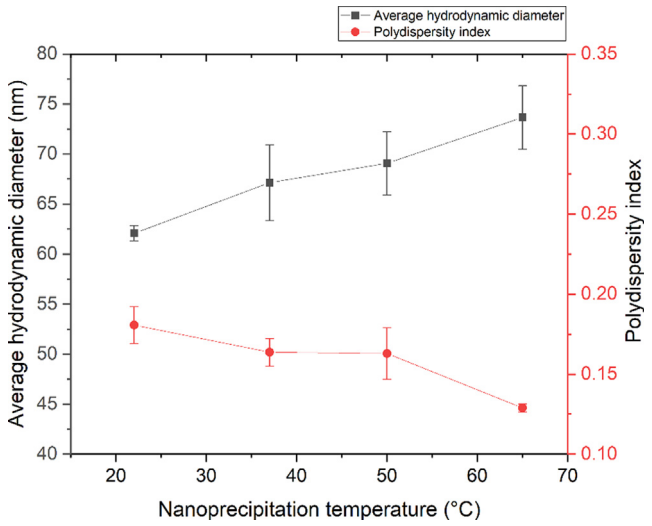

Fig. 4. Effect of nanoprecipitation temperature on average hydrodynamic diameter and polydispersity index. The data is from three complete repetitions of the experiment. Average values ± SD are shown.

Re (*e.g.*, d_H = 62.7 ± 0.5 nm and PDI = 0.135 ± 0.013 at 140 Re). The flow rate region of 30–150 Re seemed stable in terms d_H, PDI and ζ-potential. Qualitatively, these observations regarding flow rate are consistent with the current understanding of the nanoprecipitation of diblock copolymers, using the diffusion-limited coalescence model. Low flow rates inside a micromixer result in slow mixing of the solvent and antisolvent phases. If the corresponding mixing time is larger than the characteristic time associated with the coalescence process, the process will be dominated by particle growth through the addition of individual polymer chains into existing nuclei, resulting in large average particle size [25,28]. Conversely, if mixing times are low compared to the characteristic time, high supersaturation is achieved rapidly throughout the sample and the formation of nuclei and cluster-to-cluster aggregation are the dominant mechanisms for particle formation [25]. As the nuclei are stabilized at certain aggregation number by steric effect of the hydrated PEG chains, a population of small, homogeneous NPs is obtained at high supersaturation values (at high Re) [60]. When mixing time is below the characteristic time, particle size will not decrease further with increased mixing speed, which can be seen here as plateauing of particle size and PDI at above ~ 30 Re in Fig. 2**F** and later in section 3.5, and this behavior is consistent with earlier reports on microfluidic nanoprecipitation [61].

Next, we studied the effect of nanoprecipitation temperature in more detail, by performing three complete repetitions of the experiment to account for batch-to-batch variation. The effect of temperature on particle size distribution is summarized in Fig. 4. Increasing the process temperature from + 20 to + 65 °C increased the average hydrodynamic diameter and reduced the PDI significantly. Increasing the nanoprecipitation temperature improves mixing of the fluids by reduction of viscosity and increase in diffusivity, which is expected to reduce PDI.

An increase in PEG-*b*-PCL particle size as a function of nanoprecipitation temperature was reported by Zhou *et al.* when THF was used as the organic solvent and it was shown to correspond with the formation of vesicles [20]. They hypothesized that evaporation (boiling) of the organic solvent assists in the self-assembly process through bubble formation. In the present work, boiling of acetone was detected within the micromixer at 50 °C and 65 °C, which may indeed modify the flow patterns inside the micromixer and the resulting microbubbles may influence copolymer self-assembly. However, no major differences were seen in the particle morphology as a function of nanoprecipitation temperature by Cryo-TEM, as a mixture of spheres and worm-like structures was seen in samples prepared at + 22 °C and + 65 °C (**Fig. S5**, Runs 25 and 28 in **Table S2**).

Interestingly, substantial batch-to-batch variation was observed in sorafenib encapsulation even though particle size, PDI and ζ-potential data remained very consistent between parallel batches (**Fig. S6** C–D). Poor encapsulation was also clearly visible as the formation of SFB precipitate inside the dialysis bag during the solvent removal process. In light of this variation, the loading degree and encapsulation efficiency data corresponding to the data points in Fig. 2 were discarded.

3.4. Effects of different solvent removal methods

As discussed, substantial batch-to-batch variation was observed in sorafenib encapsulation when using the microfluidic process with dialysis-based solvent removal. Formation of crystalline SFB precipitate was evident from visual examination of several of the dialyzed samples and corresponded with low encapsulation efficiency values. We hypothesized that this inconsistent loading may be due to premature drug release during the solvent removal process due to different rates of solvent removal between the methods. To test this hypothesis, several trial runs were performed using different sample collection and solvent removal techniques.

For each experimental run, 4.0 mL of sample was prepared by the microfluidic method, using the default parameter values in **Table S1**. The sample was collected either into an empty container (*non-dilutive*) or into 20 mL of ion-exchange water (*dilutive*), in order to see if an increase in water-to-acetone ratio could retard the hypothesized premature drug release, and solvent removal was started immediately. Three different methods were used for solvent removal: dialysis, TFF or evaporation (as detailed in Methods). After solvent removal, regardless of the method used, samples were filtered using 0.45 μm syringe filters (Cellulose acetate, VWR). Three full repetitions of the experiment were performed. The data is presented in Fig. 5.

Important differences can be seen between samples prepared using different purification methods. Firstly, the evaporation method yielded significantly smaller particles than the other methods (Fig. 5A). No major differences were observed in ζ-potential or PDI values (Fig. 5B,C). As expected from the earlier experiments, substantial variation in drug loading was seen in the dialyzed samples, with drug loading varying between 11.7 % and 0.8 % between parallel batches (Fig. 5D). Solvent removal by evaporation resulted in systematically very low final loading degrees (between 0.7 and 0.9 %). No clear differences between dilutive and non-dilutive sample collection could be observed. Interestingly, drug loading remained the most consistent (between 7.1 and 10.4 %) from batch-to-batch when the TFF method was applied.

We hypothesize that these differences in final loading degree between samples prepared with different solvent removal methods are due to different rates of solvent removal. After nanoprecipitation of drug-loaded NPs, the dispersing solution will be supersaturated with drug. If the drug itself starts to precipitate out from the solution as crystals, supersaturation level will be reduced and drug diffusion will be able occur from NPs into solution more rapidly due to the higher concentration gradient. Additionally, if this precipitation of crystalline drug starts when solvent concentration remains elevated, the drug solubility and the rate of drug diffusion will be high, and thus, the drug will be able to diffuse out from the NP rapidly.

For example, in the case of the evaporation method, the samples were placed in open glass vials with magnetic stirring at room temperature. In such a setup, the rate of solvent removal is expected to be slow compared to TFF. Similarly, the equilibration

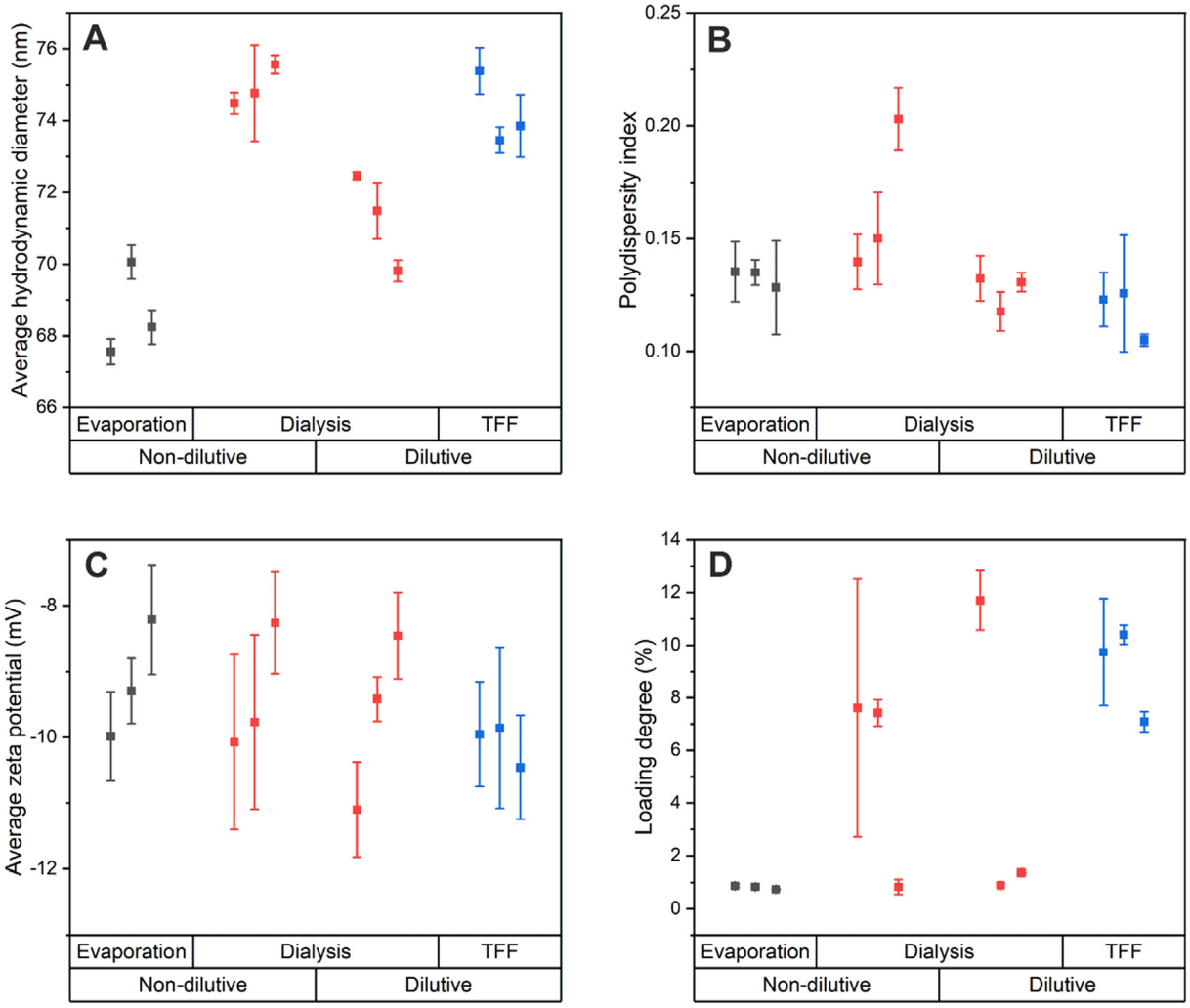

Fig. 5. Effects of different NP collection methods (dilutive and non-dilutive) and acetone removal methods (evaporation, dialysis and tangential flow filtration) on the hydrodynamic diameter (A), polydispersity index (B), ζ-potential (C) and SFB loading degree (D) of purified NPs. Average values ± SD (n = 3) are shown for three parallel batches were prepared per condition.

of a dialysis system takes several hours (as shown also later in section 3.7) and the entire dialysis process lasted 48 h, whereas for TFF, the entire process lasted ~ 1 h. Furthermore, dialysis method offers poor control over the rate of solvent exchange, as the rate may depend on multiple factors, such as stirring efficiency, tightness of the seal of the dialysis bag, and bag surface area.

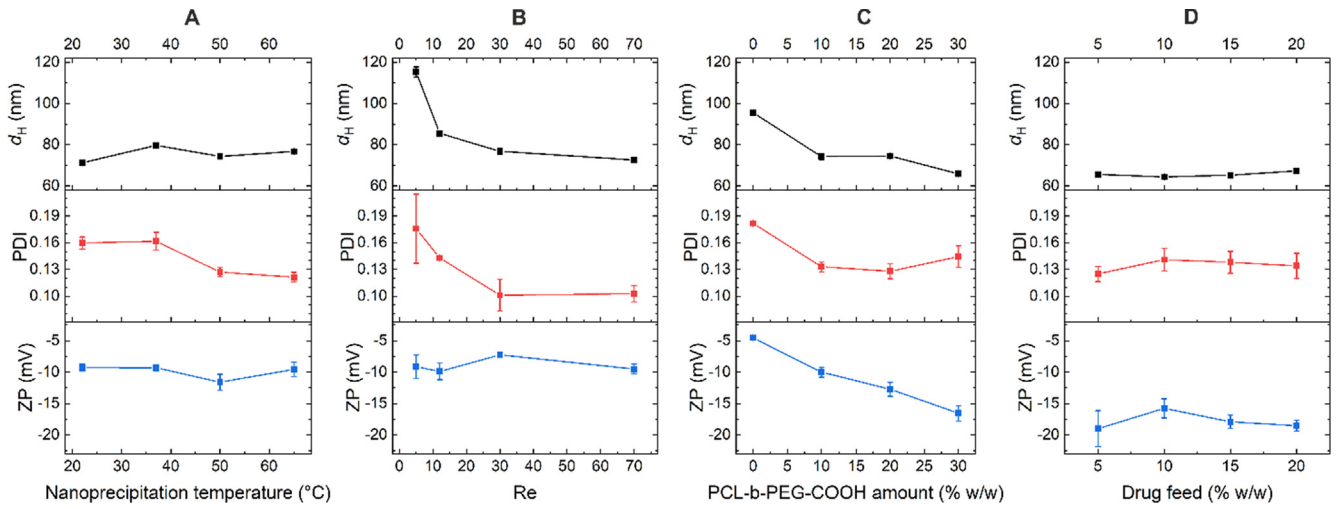

Fig. 6. The effects of nanoprecipitation temperature (A), Reynolds number (B), PCL-*b*-PEG-COOH amount (C) and sorafenib feed (D) on average hydrodynamic diameter, PDI and ζ-potential on the PEG-*b*-PCL NPs. Average values ± SD (n = 3) from single batches per condition are shown.

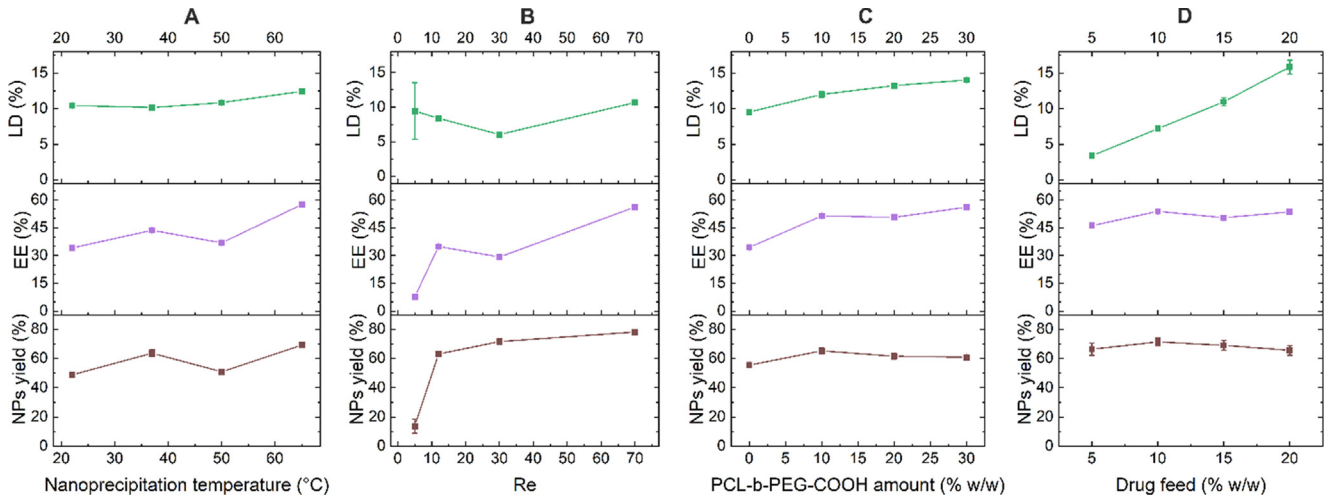

Fig. 7. The effects of nanoprecipitation temperature (A), Reynolds number (B), PCL-*b*-PEG-COOH amount (C) and sorafenib feed (D) on sorafenib loading degree (LD%), encapsulation efficiency (EE%) and total yield of PEG-*b*-PCL NPs (NPs yield %). Average values ± SD (n = 3) from single batches per condition are shown.

Therefore, it is conceivable that the high final loading degrees obtained with TFF based purification were enabled by rapid solvent removal, which prevented fast premature release of SFB from the NPs. However, further investigation would be needed to confirm whether drug precipitation as crystals started only during the solvent removal process or if a population of nanocrystals formed already during the microfluidic step. Regardless of the underlying mechanism, using TFF-based purification was useful in consistently obtaining a high final SFB loading degree.

3.5. Effects of the formulation and microfluidic process parameters: TFF-based solvent removal experiments

Selected optimization experiments were repeated, implementing the TFF method to reduce batch-to-batch variability in drug loading. Nanoparticles were prepared as previously described, with the exception that 8 mL of dispersion was collected from the micromixer outlet into 40 mL of ion-exchange water and the solvent was removed by tangential flow filtration using the protocol shown in the Methods. A full list of nanoprecipitation parameters is available in **Table S3**. Finally, the samples were filtered using 0.45 μm syringe filters, similarly to all previous experiments.

Data obtained using the TFF-based process are summarized in Figs. 6 and 7. It is worth noting that only a single batch per treatment condition was prepared. It should also be mentioned that because the manufactured batch size was small compared to the maximum capacity of the TFF apparatus, loss of nanoparticles unavoidably occurred in the filtration cassette and tubing, which limited the maximum attainable NPs yield. Furthermore, it should be understood that the calculated encapsulation efficiency is also affected by this limited yield and thus slightly higher EE and yield values are expected to be obtained with larger batch sizes.

Similarly to the dialysis-based method, increasing the nanoprecipitation temperature reduced PDI significantly (from 0.160 ± 0.007 to 0.121 ± 0.006), whereas the effects of temperature on d_H and ζ-potential were negligible (Fig. 6A). Loading degree was significantly improved by increasing the nanoprecipitation temperature and encapsulation efficiency and NPs yield also showed a small positive trend with increasing temperature (Fig. 7A).

As previously seen with the dialysis-based process, fluid flow rate had a strong effect on d_H and PDI, indicating that larger and less homogeneous particles are obtained at low Re (Fig. 6B). Furthermore, low Re resulted in minimal yield (13.7 ± 4.9 %) and encapsulation efficiency (7.7 ± 0.1 %) values (Fig. 7B), suggesting that due to poor mixing, significant part of the polymer was not able to self-assemble into nanoparticles, but may have rather formed larger aggregates or precipitate that was removed during the syringe filtration step. This hypothesis is supported by the significantly higher d_H and PDI at low Re. These observations are expected for nanoprecipitation in a micromixer device, as faster flow improves the mixing efficiency (see 3.2 for discussion). The maximum flow rate studied (Re = 140) corresponded to 387.5 mL/h total device output.

As expected, ζ-potential of the NPs decreased linearly with the amount of added PCL-*b*-PEG-COOH (Fig. 6C). Increasing the amount of PCL-*b*-PEG-COOH also reduced strongly the d_H and PDI, which can be explained by electrostatic repulsion of the corona-forming blocks, as described above. Increasing the drug feed did not markedly affect d_H, PDI or ζ-potential (Fig. 6D). Loading of sorafenib increased linearly with increasing drug feed up to a LD value of 15.9 ± 1.0 % at 30 % drug feed, and EE (%) and NPs yield remained remarkably constant with increasing drug feed values. This suggest that even higher loading values could be obtained by the present method by increasing the drug feed further.

3.6. Drug solubilization

Solubility values obtained for SFB in phosphate and acetate buffers at different pH with and without FBS supplementation are shown in Figure S8. For example, SFB solubility in PBS at pH 7.4 was determined to be 7.9 ± 0.9 μg/L. Since a 1.0 mg/mL dispersion of NPs at 15.9 % loading corresponds to 159000 μg/L drug, the achieved drug loading indicates a ~ 20000-fold improvement in aqueous solubility. For comparison, previous work by Letchford et al. on PEG-*b*-PCL micelles reported a 1068-fold and 130100-fold solubility improvements for paclitaxel and curcumin, respectively [62].

3.7. Stability of NPs in water over storage

Results from the stability study are shown in Fig. 8. The average d_H and PDI remained constant for the 4-month study period at both + 7 °C and + 25 °C, indicating high colloidal stability of the PEG-*b*-PCL NPs as an aqueous dispersion (Fig. 8A–B). Colloidal stability of these particles is expected due to their small size and the steric stabilization effect of the PEGylated surface. However, as seen in Fig. 8C, SFB content of the NPs decreased rapidly upon storage, with a two-week drug loss of approximately 48 % at + 7 °C and 79 % at + 25 °C. This behavior is likely due to the small size of the NPs and the ability of this small

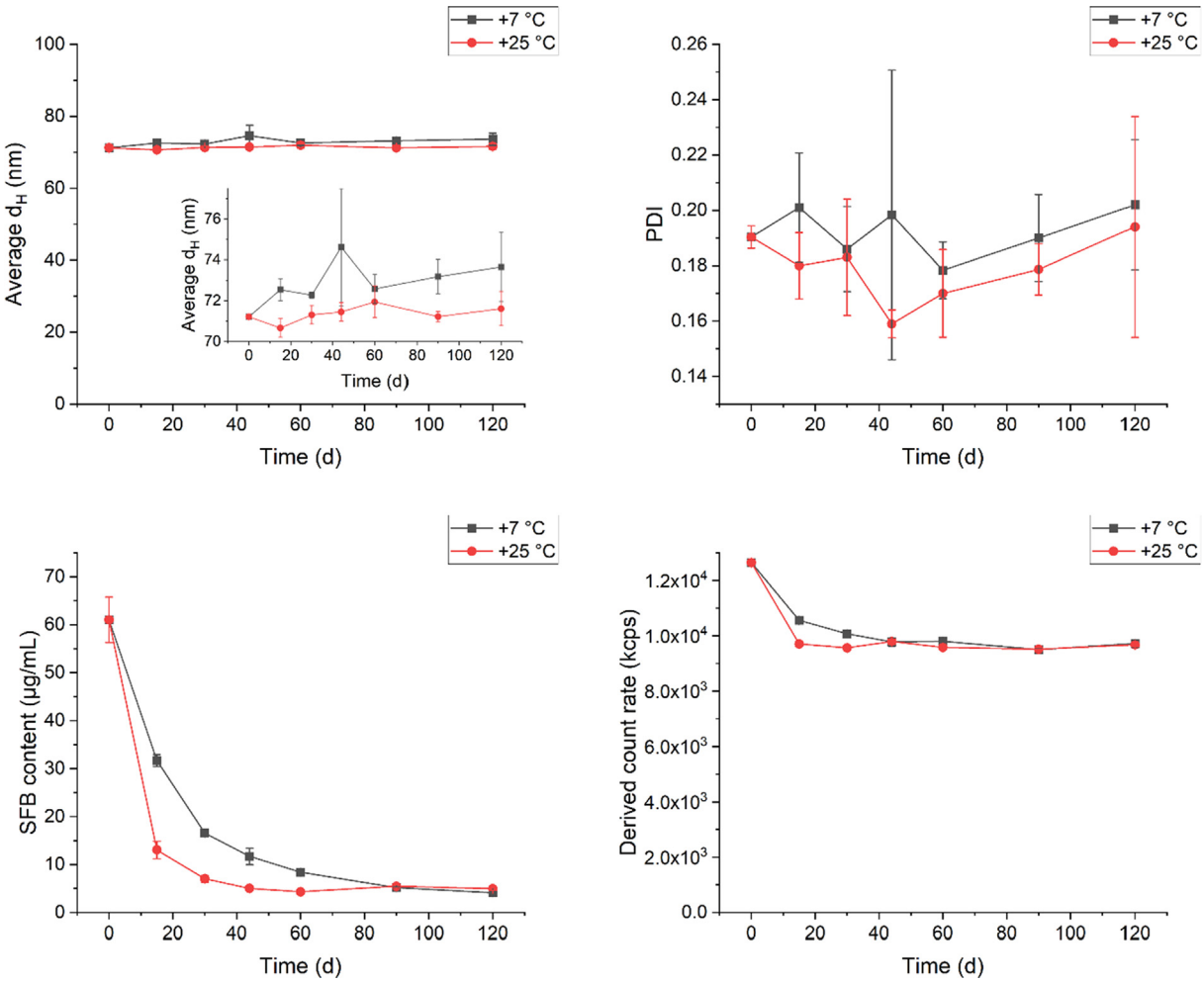

Fig. 8. Stability data of the aqueous dispersion sorafenib-loaded PEG-*b*-PCL NPs. Average values ± SD from three repeat measurements on a single sample are shown per time point.

hydrophobic drug to diffuse in the polymer matrix. Light microscopy investigation of the centrifuged stability samples revealed a large population drug crystals in the pellet (Fig. S7).

Because particle size remained practically unchanged, it is possible to evaluate changes in particle concentration by scattering intensity, which was accomplished by plotting the *derived count rate* values calculated by the Zetasizer software (Fig. 8D). The data shows an initial drop in particle concentration, which correlates well with the reduction in SFB content at each temperature, followed by a stable plateau with no further reduction detected within the 4-month experiment. This suggests that no significant degradation of PCL occurred during the study, as the degradation would be expected to reduce particle size and concentration.

Collectively, these results suggest that the particles did not significantly agglomerate or degrade during 4 months of storage in ion-exhange water at + 7 °C and + 25 °C. However, the majority of the loaded drug released within weeks of storage, suggesting that the loading of sorafenib was thermodynamically unstable and likely controlled by diffusion in the polymer matrix. Lyophilization of the formulation could be considered to improve storage stability [63].

3.8. Sorafenib release rate in vitro

Release rate of sorafenib from the optimized formulation, prepared with the TFF-based method, was analyzed in PBS pH 5.5 and pH 7.4 supplemented with 10 % FBS. To allow rational design of the experiment, the solubility of SFB in the release media was first determined. The obtained solubility data in PBS and acetate buffers shown in **Figure S8** demonstrate that solubility was increased significantly by the addition of 10 % FBS into the dissolution medium. For example, the drug solubility at PBS pH 7.4 was determined to be 7.9 ± 0.9 µg/L without FBS and 321 ± 22 µg/L with FBS. For dissolution and drug release testing, sink conditions should be ensured, which can be achieved by having at least 3–10 times larger dissolution volume than the saturation volume [57,64]. To meet this condition, initial amount of drug inside the dialysis bag was adjusted to 25 ± 2 µg for all experiments, corresponding to one third of SFB solubility in 300 mL of PBS pH 7.4 + 10 % FBS. Further increases in dissolution volume would result in analytical difficulties due to extremely low final concentrations in medium.

Results of the release rate experiments are shown in Fig. 9. The data demonstrates clearly that sorafenib was released from the PEG-*b*-PCL NPs in a sustained manner compared to the solution control, with 13.6 ± 9.0 % released in 8 h and 25.3 ± 22.7 % released in 24 h from the NPs at pH 7.4. The drug release rate was not significantly dependent on the pH-values tested. High standard deviations of the release values are likely due to losses in the diethyl ether extraction process. Precipitation of protein at the water-organic interface rendered the efficient separation of the two phases difficult, causing variation in extraction efficiency.

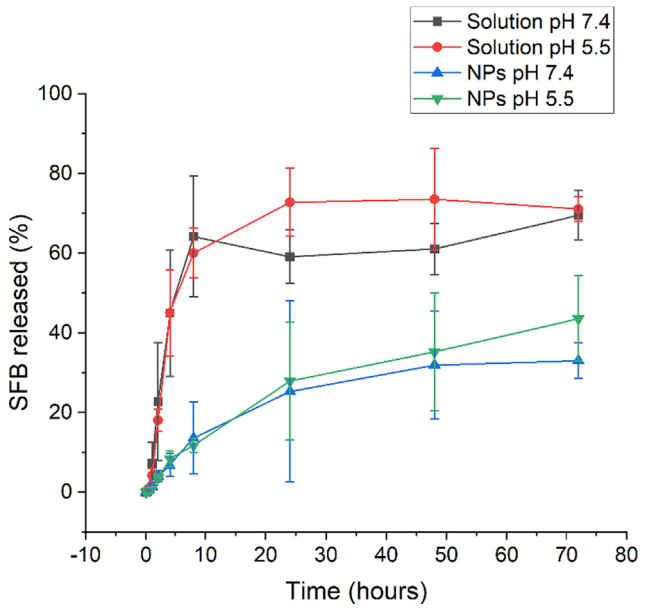

Fig. 9. SFB release profiles of PEG-*b*-PCL NPs in 1X PBS at pH 7.4 and pH 5.5 supplemented with 10 % of FBS. Sorafenib solutions in PEG400:water (1:1) are included as control samples to illustrate the diffusion delay of the dialysis bag method. Average values ± SD from three complete repetitions of the experiment are shown.

Release from the control samples (drug solution) stabilized at ~ 70 %, which was likely caused by limited yield of the extraction step, since the solubility analyses confirmed that sink conditions were obeyed. Furthermore, the analysis of dialysis bags contents at 72 h (**Figure S9**) showed that a complete release (over 99 %) of SFB was achieved for the control samples, which suggests that the limited release values in Fig. 9 were mainly due to losses during the extraction step and not due to limited solubility in release medium.

Binding of SFB to the dialysis membrane was quantified by acetone extraction, in a similar separate experiment, details of which are available in Supplementary Information, to be 0.34 ± 0.13 μg, which is 1.4 % of the total amount of drug in the dialysis system of the present experiment. This indicates, that at very low release percentages, binding of SFB may constitute a significant source of error. This corresponds with the small delay in the initial rise of release values, which can also be seen when looking at the early time points in Fig. 9 and in more detail in Figure S10. Another factor contribution to this delay may be the finite time required for SFB to diffuse inside the membrane to establish the concentration gradient and to reach the outside surface.

It is also noteworthy that there was a significant overall time delay associated with the dialysis bag method, as full equilibration of the system for the control samples took several hours (Fig. 9), which is not expected for the actual *in vivo* application scenario of intravenous injection of a drug solution, where fast mixing will take place due to blood flow. Even though the dialysis bag method is the most widely utilized release rate analysis technique for nanoparticulate systems [57], it has several drawbacks. Besides the diffusional barrier caused by the dialysis membrane, another important consideration is that the environment the sample experiences is markedly different in the dialysis bag compared to the human bloodstream, as the inside and outside compartments remain separated and no mechanical mixing occurs inside the dialysis bag.

These inherent limitations of the method may cause difficulties in accurate prediction of release *in vivo* based on *in vitro* data. Therefore, further development of the analytical method should be considered and other methodologies with higher *in vitro–in vivo* correlation should be explored, as well as using different release media, such as blood plasma. Nevertheless, taking the limitations into account, the method showed clearly that the NPs released the drug in a sustained manner over several days, which is desirable for reducing the drug-related side effects caused by fluctuations in free drug concentration and minimizing the required frequency of injections.

4. Conclusions

In this work, a microfluidic process was developed and optimized for the controlled preparation of PEG-*b*-PCL NPs loaded with sorafenib free base, intended for i.v. administration for cancer therapy applications. The highly hydrophobic drug was successfully solubilized, with up to 16 ± 1 % loading degree at 54 ± 1 % encapsulation efficiency, corresponding to ~ 20000-fold increase in solubility as compared to free drug in PBS. The optimized formulation exhibited spherical morphology, small particle size (d_H < 80 nm) and uniform size distribution (PDI < 0.2). Overall, the developed formulation demonstrated sustained drug release over several days *in vitro* and the NPs showed high colloidal stability in water.

We showed that particle size distribution, morphology, ζ-potential and sorafenib loading could be effectively controlled by adjusting the formulation and process parameters. Notably, the addition of carboxylic acid functionalized polymer was useful in driving the morphology distribution towards solid spherical particles, reducing the PDI and improving the drug loading. In addition, the process temperature and flow rate had the largest effects on formulation properties within the ranges explored. It was shown that increasing the nanoprecipitation temperature resulted in increased drug loading, increased mean particle size and reduced PDI. An optimal region of fluid flow rate was identified to maximize process yield and minimize PDI.

Interestingly, the choice of organic solvent removal method had a strong effect on the final encapsulation efficiency. This effect was attributed to different rates of organic solvent removal from the dispersion. When combined with tangential flow filtration, the microfluidic process allowed a precise control over NP's properties, and showed high yield and batch-to-batch reproducibility. The optimized process was fast, as the complete production of a development batch from preparation of initial solutions to final syringe filtration was possible in<3 h. In conclusion, we have presented a feasible and well-controlled process for the preparation of sorafenib-loaded PEG-*b*-PCL nanoparticles, potentially applicable also for different drug-polymer combinations.

Notes. *V. Känkänen and V. Balasubramanian are employees at Bayer Oy (Finland). The other authors declare no conflict of interest.*

CRediT authorship contribution statement

Voitto Känkänen: Conceptualization, Methodology, Investigation, Formal analysis, Visualization, Writing – original draft. **Micaela Fernandes:** Investigation. **Zehua Liu:** Methodology, Writing – review & editing. **Jani Seitsonen:** Investigation. **Sami-Pekka Hirvonen:** Investigation, Writing – review & editing. **Janne Ruokolainen:** Resources, Supervision. **João F. Pinto:** Supervision, Writing – review & editing. **Jouni Hirvonen:** Supervision, Writing – review & editing. **Vimalkumar Balasubramanian:** Conceptualization, Funding acquisition, Supervision, Writing – review & editing. **Hélder A. Santos:** Supervision, Resources, Funding acquisition, Project administration, Conceptualization, Writing - review & editing.

Data availability

Data will be made available on request.

Declaration of Competing Interest

The authors declare that they have no known competing financial interests or personal relationships that could have appeared to influence the work reported in this paper.

Acknowledgements

V. Känkänen and H.A. Santos acknowledge Bayer Oy (Finland) for financial support. H.A. Santos acknowledges also the Sigrid Jusélius Foundation and the UMCG Research Fund for financial support.

Appendix A. Supplementary material

Supplementary data to this article can be found online at https://doi.org/10.1016/j.jcis.2022.11.124.

References

[1] Y. Mai, A. Eisenberg, Self-assembly of block copolymers, Chem. Soc. Rev. 41 (18) (2012) 5969.
[2] M.L. Adams, A. Lavasanifar, G.S. Kwon, Amphiphilic block copolymers for drug delivery, J. Pharm. Sci. 92 (7) (2003) 1343–1355.
[3] V.P. Bharti et al., Strategies to enhance solubility and dissolution of a poorly water soluble drug, J. Innovations in Pharmaceuticals and Biol. Sci. 2 (4) (2015) 482–494.
[4] J. Szebeni, C.R. Alving, F.M. Muggia, Complement Activation by Cremophor EL as a possible contributor to hypersensitivity to paclitaxel: an in vitro study, JNCI: J. National Cancer Institute 90 (4) (1998) 300–306.
[5] D.L. Stirland, J.W. Nichols, S. Miura, Y.H. Bae, Mind the gap: a survey of how cancer drug carriers are susceptible to the gap between research and practice, J. Control. Release 172 (3) (2013) 1045–1064.
[6] A. Gagliardi, E. Giuliano, E. Venkateswararao, M. Fresta, S. Bulotta, V. Awasthi, D. Cosco, Biodegradable polymeric nanoparticles for drug delivery to solid tumors, Front. Pharmacol. 12 (2021).
[7] R. Duncan, M.J. Vicent, Polymer therapeutics-prospects for 21st century: the end of the beginning, Adv. Drug Deliv. Rev. 65 (1) (2013) 60–70.
[8] H. Maeda, Toward a full understanding of the EPR effect in primary and metastatic tumors as well as issues related to its heterogeneity, Adv. Drug Deliv. Rev. 91 (2015) 3–6.
[9] Y. Matsumura, H. Maeda, A new concept for macromolecular therapeutics in cancer chemotherapy: mechanism of tumoritropic accumulation of proteins and the antitumor agent smancs, Cancer Res. 46 (12 Part 1) (1986) 6387.
[10] R. Bazak, M. Houri, S. El Achy, S. Kamel, T. Refaat, Cancer active targeting by nanoparticles: a comprehensive review of literature, J. Cancer Res. Clin. Oncol. 141 (5) (2015) 769–784.
[11] B. Bahrami, M. Hojjat-Farsangi, H. Mohammadi, E. Anvari, G. Ghalamfarsa, M. Yousefi, F. Jadidi-Niaragh, Nanoparticles and targeted drug delivery in cancer therapy, Immunol. Lett. 190 (2017) 64–83.
[12] M.A. Woodruff, D.W. Hutmacher, The return of a forgotten polymer—Polycaprolactone in the 21st century, Prog. Polym. Sci. 35 (10) (2010) 1217–1256.
[13] M.V. Christen, F., Polycaprolactone: or how a well-known and futuristic polymer has become an innovative collagen-stimulator in esthetics, Clin. Cosmet. Investig. Dermatol. 13 (2020) 31–48.
[14] H. Schellekens, W.E. Hennink, V. Brinks, The immunogenicity of polyethylene glycol: facts and fiction, Pharm. Res. 30 (7) (2013) 1729–1734.
[15] Z. Binkhathlan, W. Qamar, R. Ali, H. Kfoury, M. Alghonaim, Toxicity evaluation of methoxy poly(ethylene oxide)-block-poly(ε-caprolactone) polymeric micelles following multiple oral and intraperitoneal administration to rats, Saudi Pharmaceutical J. 25 (6) (2017) 944–953.
[16] R.P, Bulcão, et al., *Acute and Subchronic Toxicity Evaluation of Poly(ε-Caprolactone) Lipid-Core Nanocapsules in Rats.* Toxicological Sciences, 2013. **132**(1): p. 162-176.
[17] C.Y. Gong, Q.J. Wu, P.W. Dong, S. Shi, S.Z. Fu, G. Guo, H.Z. Hu, X. Zhao, Y.Q. Wei, Z.Y. Qian, Acute toxicity evaluation of biodegradable in situ gel-forming controlled drug delivery system based on thermosensitive PEG-PCL-PEG hydrogel, J. Biomed. Mater. Res. B Appl. Biomater. 91B (1) (2009) 26–36.
[18] R.S. Bezwada, D.D. Jamiolkowski, I.-Y. Lee, V. Agarwal, J. Persivale, S. Trenka-Benthin, M. Erneta, J. Suryadevara, A. Yang, S. Liu, Monocryl suture, a new ultra-pliable absorbable monofilament suture, Biomaterials 16 (15) (1995) 1141–1148.
[19] D.J. Adams, C. Kitchen, S. Adams, S. Furzeland, D. Atkins, P. Schuetz, C.M. Fernyhough, N. Tzokova, A.J. Ryan, M.F. Butler, On the mechanism of formation of vesicles from poly(ethylene oxide)-block-poly(caprolactone) copolymers, Soft Matter 5 (16) (2009) 3086.
[20] J. Zhou, R. Ni, Y. Chau, Polymeric vesicle formation via temperature-assisted nanoprecipitation, RSC Adv. 7 (29) (2017) 17997–18000.
[21] Z.-X. Du, J.-T. Xu, Z.-Q. Fan, Regulation of micellar morphology of PCL-b-PEO block copolymers by crystallization temperature, Macromol. Rapid Commun. 29 (6) (2008) 467–471.
[22] T. Zou, F. Dembele, A. Beugnet, L. Sengmanivong, S. Trepout, S. Marco, A.d. Marco, M.-H. Li, Nanobody-functionalized PEG-b-PCL polymersomes and their targeting study, J. Biotechnol. 214 (2015) 147–155.
[23] Y. Geng, P. Dalhaimer, S. Cai, R. Tsai, M. Tewari, T. Minko, D.E. Discher, Shape effects of filaments versus spherical particles in flow and drug delivery, Nat. Nanotechnol. 2 (4) (2007) 249–255.
[24] I.A.B. Pijpers, L.K.E.A. Abdelmohsen, Y. Xia, S. Cao, D.S. Williams, F. Meng, J.C.M. Hest, Z. Zhong, Adaptive polymersome and micelle morphologies in anticancer nanomedicine: from design rationale to fabrication and proof-of-concept studies, Advanced Therapeutics 1 (8) (2018) 1800068.
[25] Y. Liu, G. Yang, D.a. Zou, Y. Hui, K. Nigam, A.P.J. Middelberg, C.-X. Zhao, Formulation of nanoparticles using mixing-induced nanoprecipitation for drug delivery, Ind. Eng. Chem. Res. 59 (9) (2020) 4134–4149.
[26] C.J. Martínez Rivas, M. Tarhini, W. Badri, K. Miladi, H. Greige-Gerges, Q.A. Nazari, S.A. Galindo Rodríguez, R.Á. Román, H. Fessi, A. Elaissari, Nanoprecipitation process: from encapsulation to drug delivery, Int. J. Pharm. 532 (1) (2017) 66–81.
[27] Z. Liu et al., Microfluidics for production of particles: mechanism, methodology, and applications, Small 16 (2020) 1904673.
[28] P.M. Valencia, O.C. Farokhzad, R. Karnik, R. Langer, Microfluidic technologies for accelerating the clinical translation of nanoparticles, Nat. Nanotechnol. 7 (10) (2012) 623–629.
[29] U.M. Attia, S. Marson, J.R. Alcock, Micro-injection moulding of polymer microfluidic devices, Microfluid. Nanofluid. 7 (1) (2009) 1–28.
[30] B. Herranz-Blanco, E. Ginestar, H. Zhang, J. Hirvonen, H.A. Santos, Microfluidics platform for glass capillaries and its application in droplet and nanoparticle fabrication, Int. J. Pharm. 516 (1-2) (2017) 100–105.
[31] G.M. Whitesides, The origins and the future of microfluidics, Nature 442 (7101) (2006) 368–373.
[32] B. Herranz-Blanco, D. Liu, E. Mäkilä, M.-A. Shahbazi, E. Ginestar, H. Zhang, V. Aseyev, V. Balasubramanian, J. Salonen, J. Hirvonen, H.A. Santos, On-chip self-assembly of a smart hybrid nanocomposite for antitumoral applications, Adv. Funct. Mater. 25 (10) (2015) 1488–1497.
[33] D. Liu, C.R. Bernuz, J. Fan, W. Li, A. Correia, J. Hirvonen, H.A. Santos, A Nano-in-nano vector: merging the best of polymeric nanoparticles and drug nanocrystals, Adv. Funct. Mater. 27 (9) (2017) 1604508.
[34] D. Liu, S. Cito, Y. Zhang, C.-F. Wang, T.M. Sikanen, H.A. Santos, A Versatile and robust microfluidic platform toward high throughput synthesis of homogeneous nanoparticles with tunable properties, Adv. Mater. 27 (14) (2015) 2298–2304.
[35] D. Liu, H. Zhang, S. Cito, J. Fan, E. Mäkilä, J. Salonen, J. Hirvonen, T.M. Sikanen, D.A. Weitz, H.A. Santos, Core/shell nanocomposites produced by superfast sequential microfluidic nanoprecipitation, Nano Lett. 17 (2) (2017) 606–614.
[36] I. Arduino, Z. Liu, A. Rahikkala, P. Figueiredo, A. Correia, A. Cutrignelli, N. Denora, H.A. Santos, Preparation of cetyl palmitate-based PEGylated solid lipid nanoparticles by microfluidic technique, Acta Biomater. 121 (2021) 566–578.
[37] EMA, *European public assessment report (EPAR) for Nexavar - Annex 1 - Summary of product characteristics.* 2021.
[38] S.M, Wilhelm, et al., BAY 43-9006 Exhibits Broad Spectrum Oral Antitumor Activity and Targets the RAF/MEK/ERK Pathway and Receptor Tyrosine Kinases Involved in Tumor Progression and Angiogenesis. Cancer Research, 2004. **64** (19): p. 7099.
[39] E, Galanis, et al., Phase II Study of Bevacizumab in Combination with Sorafenib in Recurrent Glioblastoma (N0776): A North Central Cancer Treatment Group Trial. Clin Cancer Res, 2013. **19**(17): p. 4816.
[40] M.D. Siegelin, C.M. Raskett, C.A. Gilbert, A.H. Ross, D.C. Altieri, Sorafenib exerts anti-glioma activity in vitro and in vivo, Neurosci. Lett. 478 (3) (2010) 165–170.
[41] J.D. Hainsworth, T. Ervin, E. Friedman, V. Priego, P.B. Murphy, B.L. Clark, R.E. Lamar, Concurrent radiotherapy and temozolomide followed by temozolomide and sorafenib in the first-line treatment of patients with glioblastoma multiforme, Cancer 116 (15) (2010) 3663–3669.
[42] G. Bronte, D. Andreis, S. Bravaccini, R. Maltoni, L. Cecconetto, A. Schirone, A. Farolfi, A. Fedeli, P. Serra, C. Donati, D. Amadori, A. Rocca, Sorafenib for the treatment of breast cancer, Expert Opin. Pharmacother. 18 (6) (2017) 621–630.
[43] N. Pecuchet et al., Sorafenib in advanced melanoma: a critical role for pharmacokinetics?, Br J. Cancer 107 (3) (2012) 455–461.
[44] L. Paz-Ares, V. Hirsh, L.i. Zhang, F. de Marinis, J.-H. Yang, H.A. Wakelee, T. Seto, Y.-L. Wu, S. Novello, E. Juhász, O. Arén, Y. Sun, T. Schmelter, T.J. Ong, C. Peña, E. F. Smit, T.S. Mok, Monotherapy Administration of Sorafenib in Patients With Non-Small Cell Lung Cancer (MISSION) Trial: A Phase III, Multicenter, Placebo-Controlled Trial of Sorafenib in Patients with Relapsed or Refractory Predominantly Nonsquamous Non–Small-Cell Lung Cancer after 2 or 3 Previous Treatment Regimens, J. Thorac. Oncol. 10 (12) (2015) 1745–1753.
[45] N. d'Avanzo et al., LinTT1 peptide-functionalized liposomes for targeted breast cancer therapy, Int. J. Pharm. 597 (2021) 120346.

[46] T. Feczkó, G. Merza, G. Babos, B. Varga, E. Gyetvai, L. Trif, E. Kovács, R. Tuba, Preparation of cubic-shaped sorafenib-loaded nanocomposite using well-defined poly(vinyl alcohol alt-propenylene) copolymer, Int. J. Pharm. 562 (2019) 333–341.
[47] J. Zhang, J. Hu, H.F. Chan, M. Skibba, G. Liang, M. Chen, iRGD decorated lipid-polymer hybrid nanoparticles for targeted co-delivery of doxorubicin and sorafenib to enhance anti-hepatocellular carcinoma efficacy, Nanomed. Nanotechnol. Biol. Med. 12 (5) (2016) 1303–1311.
[48] M. Sang, R. Luo, Y. Bai, J. Dou, Z. Zhang, F. Liu, F. Feng, J. Xu, W. Liu, Mitochondrial membrane anchored photosensitive nano-device for lipid hydroperoxides burst and inducing ferroptosis to surmount therapy-resistant cancer, Theranostics 9 (21) (2019) 6209–6223.
[49] A. Clavreul, E. Roger, M. Pourbaghi-Masouleh, L. Lemaire, C. Tétaud, P. Menei, Development and characterization of sorafenib-loaded lipid nanocapsules for the treatment of glioblastoma, Drug Deliv. 25 (1) (2018) 1756–1765.
[50] M. Lei, G. Ma, S. Sha, X. Wang, H. Feng, Y. Zhu, X. Du, Dual-functionalized liposome by co-delivery of paclitaxel with sorafenib for synergistic antitumor efficacy and reversion of multidrug resistance, Drug Deliv. 26 (1) (2019) 262–272.
[51] Y. Geng, D.E. Discher, Hydrolytic Degradation of Poly(ethylene oxide)-block-Polycaprolactone Worm Micelles, J. Am. Chem. Soc. 127 (37) (2005) 12780–12781.
[52] R. Gref, A. Domb, P. Quellec, T. Blunk, R.H. Müller, J.M. Verbavatz, R. Langer, The controlled intravenous delivery of drugs using PEG-coated sterically stabilized nanospheres, Adv. Drug Deliv. Rev. 16 (2-3) (1995) 215–233.
[53] R. Gref, M. Lück, P. Quellec, M. Marchand, E. Dellacherie, S. Harnisch, T. Blunk, R.H. Müller, 'Stealth' corona-core nanoparticles surface modified by polyethylene glycol (PEG): influences of the corona (PEG chain length and surface density) and of the core composition on phagocytic uptake and plasma protein adsorption, Colloids and Surfaces B-Biointerfaces 18 (3-4) (2000) 301–313.
[54] R. Gref et al., Biodegradable long-circulating polymeric nanospheres, Science 263 (5153) (1994) 1600.
[55] Z. Liu, W. Lian, Q. Long, R. Cheng, G. Torrieri, B. Zhang, A. Koivuniemi, M. Mahmoudzadeh, A. Bunker, H. Gao, H. He, Y. Chen, J. Hirvonen, R. Zhou, Q. Zhao, X. Ye, X. Deng, H.A. Santos, Promoting cardiac repair through simple engineering of nanoparticles with exclusive targeting capability toward myocardial reperfusion injury by thermal resistant microfluidic platform, Adv. Funct. Mater. 32 (36) (2022) 2204666.
[56] V. Känkänen, J. Seitsonen, H. Tuovinen, J. Ruokolainen, J. Hirvonen, V. Balasubramanian, H.A. Santos, Evaluation of the effects of nanoprecipitation process parameters on the size and morphology of poly(ethylene oxide)-block-polycaprolactone nanostructures, Int. J. Pharm. 590 (2020) 119900.
[57] J. Shen, D.J. Burgess, In vitro dissolution testing strategies for nanoparticulate drug delivery systems: recent developments and challenges, Drug Deliv. Transl. Res. 3 (5) (2013) 409–415.
[58] S. Zhou, X. Deng, H. Yang, Biodegradable poly(ε-caprolactone)-poly(ethylene glycol) block copolymers: characterization and their use as drug carriers for a controlled delivery system, Biomaterials 24 (20) (2003) 3563–3570.
[59] A. Choucair, A. Eisenberg, Control of amphiphilic block copolymer morphologies using solution conditions, Eur. Phys. J. E 10 (1) (2003) 37–44.
[60] B.K. Johnson, R.K. Prud'homme, Mechanism for rapid self-assembly of block copolymer nanoparticles, Phys. Rev. Lett. 91 (11) (2003) 118302.
[61] J.M. Lim et al., Ultra-high throughput synthesis of nanoparticles with homogeneous size distribution using a coaxial turbulent jet mixer, ACS Nano 8 (6) (2014) 6056–6065.
[62] K. Letchford, R. Liggins, H. Burt, Solubilization of hydrophobic drugs by methoxy poly(ethylene glycol)-block-polycaprolactone diblock copolymer micelles: theoretical and experimental data and correlations, J. Pharm. Sci. 97 (3) (2008) 1179–1190.
[63] W. Abdelwahed et al., Freeze-drying of nanoparticles: Formulation, process and storage considerations, Adv. Drug Deliv. Rev. 58 (2006) 1688–1713.
[64] *5.17.1. Recommendations for dissolution testing*, in *European Pharmacopoeia*. 2016.